The Astronomical Journal, 152:59 (8pp), 2016 September doi:10.3847/0004-6256/152/3/59

MODEL-OBSERVATION COMPARISONS OF ELECTRON NUMBER DENSITIES IN THE COMA OF 67P/CHURYUMOV–GERASIMENKO DURING 2015 JANUARY

E. Vigren[1], K. Altwegg[2], N. J. T. Edberg[1], A. I. Eriksson[1], M. Galand[3], P. Henri[4], F. Johansson[1,4,5], E. Odelstad[1,5], C.-Y. Tzou[2], and X. Vallières[4]
[1] Swedish Institute of Space Physics, Uppsala, Sweden; erik.vigren@irfu.se
[2] Physikalisches Institut, University of Bern, Bern, Switzerland
[3] Department of Physics, Imperial College London, London, UK
[4] Laboratoire de Physique et Chimie de l'Environnement et de l'Espace, Orleans, France
[5] Department of Physics and Astronomy, Uppsala University, Uppsala, Sweden
Received 2016 March 28; revised 2016 May 26; accepted 2016 June 3; published 2016 August 18

ABSTRACT

During 2015 January 9–11, at a heliocentric distance of ~2.58–2.57 au, the ESA *Rosetta* spacecraft resided at a cometocentric distance of ~28 km from the nucleus of comet 67P/Churyumov–Gerasimenko, sweeping the terminator at northern latitudes of 43°N–58°N. Measurements by the *Rosetta* Orbiter Spectrometer for Ion and Neutral Analysis/Comet Pressure Sensor (ROSINA/COPS) provided neutral number densities. We have computed modeled electron number densities using the neutral number densities as input into a Field Free Chemistry Free model, assuming H_2O dominance and ion-electron pair formation by photoionization only. A good agreement (typically within 25%) is found between the modeled electron number densities and those observed from measurements by the Mutual Impedance Probe (RPC/MIP) and the Langmuir Probe (RPC/LAP), both being subsystems of the *Rosetta* Plasma Consortium. This indicates that ions along the nucleus-spacecraft line were strongly coupled to the neutrals, moving radially outward with about the same speed. Such a statement, we propose, can be further tested by observations of H_3O^+/H_2O^+ number density ratios and associated comparisons with model results.

Key words: comets: individual (67P) – molecular processes

1. INTRODUCTION

In 2014 July, at a heliocentric distance of 3.6 au, the ESA *Rosetta* spacecraft rendezvoused with its target comet 67P/Churyumov–Gerasimenko (hereafter, 67P); a Jupiter family comet with an orbital period of ~6.44 years, and with aphelion and perihelion distances of ~5.68 au and ~1.25 au, respectively. Since then, *Rosetta* has followed 67P closely (mainly at cometocentric distances from ~10 km to a few hundred km) through the pre-perihelion phase (perihelion was reached on 2015 August 13) and will continue to do so until 2016 September. The shape of the comet, with two differently sized lobes connected by a neck region, has been compared with a "rubber-duck" shape, and confirmed to be a contact binary (Massironi et al. 2015). In agreement with predictions from remote sensing (Lamy et al. 2007), 67P has an effective radius of ~1.72 km and a rotation period of 12.4 hr (Sierks et al. 2015).

In the early escort phase (2014 August and September), marked latitudinal and longitudinal differences were observed in the outgassing, both in terms of intensity and composition (Hässig et al. 2015). For northern latitudes—the summer side and most active side of the comet until equinox in 2015 May—the outgassing was H_2O dominated with peaks (and dips) occurring twice per rotation period (Hässig et al. 2015). Peak number densities were observed over the neck region of the comet (to first approximation when maximum surface area of the comet was exposed to sunlight; e.g., Bieler et al. 2015). The southern hemisphere also displayed longitudinal variations, although the intensity peaks were less elevated. Interestingly, the composition over the southern latitudes was observed to be highly variable, with CO_2 periodically being more abundant than H_2O. The dominance of CO_2 prevailed in particular when the spacecraft viewed the larger of the lobes blocking the neck region (Hässig et al. 2015; Le Roy et al. 2015).

Edberg et al. (2015), focusing on measurements from 2014 October up until 2015 March, showed that electron number densities varied with the neutral number density and argued that the plasma at the spacecraft location was predominantly produced locally, or more precisely along the comet-spacecraft line. An average $1/r$ decay in the electron number density (r being the cometocentric distance) was observed as the spacecraft performed two radial scans in 2015 February, the latter and more extended covering cometocentric distances from ~8 km to ~260 km. The link between the ambient electron and neutral number densities was further highlighted by Odelstad et al. (2015), who showed that variations in the spacecraft potential (largely dictated by the ambient electron number density) correlated with variations in the neutral number density for extended time periods when the spacecraft resided at $r \sim 30$ km in 2014 September and November and 2015 January. Seemingly, this suggests a limited influence of electric fields transporting the plasma in non-radial directions.

In the present study, we use the Field Free Chemistry Free (FFCF) model of Vigren et al. (2015a) to generate modeled electron number densities, $n_{e,model}$, directly from the neutral number densities, n_N, measured by the *Rosetta* Orbiter Spectrometer for Ion and Neutral Analysis/Comet Pressure Sensor (ROSINA/COPS, Balsiger et al. 2007). The model, including its underlying assumptions, is described in Section 2.1. In Section 2.2 we focus primarily on the time period 2015 January 9–11. Section 3 is devoted to in situ measurements of n_N and n_e associated with these dates. The electron number densities are subdivided into $n_{e,MIP}$ and $n_{e,LAP}$, depending on whether they were derived from measurements by the Mutual Impedance Probe (MIP; Trotignon et al. 2007;

Edberg et al. 2015) or the dual Langmuir Probe (LAP; Eriksson et al. 2007; Edberg et al. 2015). Both MIP and LAP are subsystems of the *Rosetta* Plasma Consortium (RPC; Carr et al. 2007), which also consists of the Ion Electron Sensor (Burch et al. 2007), the Ion Composition Analyzer (ICA; Nilsson et al. 2007), and the Fluxgate Magnetometer (MAG; Glassmeier et al. 2007). In Section 4.1 the modeled electron number densities are compared with observations. It is shown that the $n_{e,model}$ and observed electron number densities agree well (typically within 25%) almost throughout the investigated time period. This indicates that our central assumptions in the model are valid for the specified time period and the associated spacecraft location. In Section 4.2 we propose an alternative approach, based on ion-neutral chemistry, to get an idea of the validity of the assumption that the ions inward of the spacecraft location move roughly with the same speed as the neutral bulk flow. Specifically, we derive an analytical expression for the H_3O^+/H_2O^+ number density ratio, and argue that comparisons with ratios derived from the ROSINA/Double Focusing Mass Spectrometer (DFMS; Balsiger et al. 2007; Fuselier et al. 2015) can serve as an indicator on the nature of the bulk plasma flow along the comet-spacecraft line. A summary with concluding remarks and brief descriptions of model–observation comparisons at other nearby dates is given in Section 5.

2. MODEL DESCRIPTION AND INVESTIGATED TIME PERIOD

2.1. The FFCF Model and its Central Assumptions

From the FFCF model formulated in, e.g., Vigren et al. (2015a), a simple relation of the electron-to-neutral number density ratio was derived. The central assumptions and simplifications are listed below and can be regarded as the four criteria for the described FFCF model to be valid.

i. We assume a strongly H_2O-dominated coma.
ii. We assume photoionization to be the dominant (in fact the only non-negligible) ion/ionization source, and we neglect attenuation of the impinging solar EUV spectra.
iii. We consider no plasma loss through dissociative recombination, and assume that grain charging has no influence on the overall ionization balance.
iv. We assume that produced ions travel radially outward with the same speed u as the neutrals, which they stem from, and we treat the free electrons simply as preserving charge neutrality.

Strictly speaking, the FFCF notation is a bit misleading. As for the Field Free (FF) part, the model also applies in the presence of electric fields as long as the neutral number density is sufficient to omit significant ion acceleration. As for the Chemistry Free (CF) part, the model applies if electron loss by other means than transport is inefficient along the nucleus-spacecraft line (however, chemistry in the form of, e.g., ion-neutral reactions is "allowed"). The electron number density, which we will refer to as $n_{e,Model}$, at cometocentric distance r is under the four specified assumptions given by

$$n_{e,Model} = \frac{\nu_{ph} \times (r - r_C)}{u} n_N, \quad (1)$$

where r is the cometocentric distance, r_C (~2 km) is the cometary radius, u is the radial velocity of the neutrals (and ions), ν_{ph} is the photoionization frequency of H_2O, and n_N is the neutral number density at r (as derived from ROSINA/COPS measurements). Vigren et al. (2015a) applied a constant (with heliocentric distance, d) expansion velocity of 0.65 km s^{-1} and a photoionization frequency that did not account for the fact that the EUV flux changes with the Sun's ~27 days rotational period. Here we make different guesstimates/estimates of u and ν_{ph} as described below.

In this work we apply the relation $u = 0.85 \times d^{-1/2}$ km s^{-1} for the expansion velocity (Equation (3) in Cochran & Schleicher 1993). Note that for $d = 3.4$ au, the resulting $u = 0.46$ km s^{-1} is close to the lower limit of the H_2O expansion velocities estimated from MIRO measurements (Doppler shift of absorption peak) in the subsolar direction of 67P (0.47–0.59 km s^{-1}; see Biver et al. 2015). However, in this work we focus exclusively on locations above the comet's terminator for which expansion velocities are anticipated to be somewhat lower than in the subsolar direction. For the dates we focus on here—2015 January 9–11 with $d = 2.58$–2.57 au (see Section 2.2) and 2015 January 31 with $d = 2.41$ au (see Section 5)—the utilized u values are 0.53 and 0.55 km s^{-1}, respectively. Due to uncertainties in the expansion velocity u, whenever displaying modeled electron number densities, we also show values higher and lower by 30% (for 2015 January 9, such a range corresponds to expansion velocities in the range 0.37–0.69 km s^{-1}).

For the investigated dates we calculated H_2O photoionization frequencies at the comet location from the photoionization cross sections presented by Schunk & Nagy (2009) and daily averaged solar EUV spectra measured by the Thermosphere Ionosphere Mesosphere Energy and Dynamics/Solar EUV Experiment, TIMED/SEE (Level 3, see Woods et al. 2005), extrapolated in phase and distance to 67P. The obtained photoionization frequencies for 2015 January 9, 10, 11, and 31 of 1.10, 1.07, 1.05, and 1.23 $\times$ 10^{-7} s^{-1}, respectively (at the comet location), are only slightly different (lower by about 4%, 6%, 8%, and 5%, respectively) compared with values given by the simple fit against d presented as Equation (2) in Vigren et al. (2015a). Overall, the electron-to-neutral number density ratios resulting from Equation (1) with the new values of u and ν_{ph} are ~13%–18% and ~12% higher than suggested by the guiding electron-to-neutral number density ratio presented as Equation (4) in Vigren et al. (2015a) for January 9–11 and 31, respectively.

As a side note, although it is not used explicitly in this work and does not account for solar EUV variability with the Sun's 27 days rotational period, we note that the memorable expression

$$\frac{n_e}{n_N}(\text{FFCF Model}) \approx \frac{r_s}{d^{3/2}} \times 10^{-6}, \quad (2)$$

with r_s ($= r - r_C$) the distance to the cometary surface in km and d in au, can be used as a proxy for the electron-to-neutral number density ratio under the assumptions of the FFCF model. Extrapolation to other comets requires scaling to long-term variability in the solar EUV flux levels. Equation (2) is associated with an H_2O photoionization frequency at 1 au of ~7 $\times$ 10^{-7} s^{-1}.

2.2. Investigated Time Period

We identified 2015 January 9–11 as a time period that is suitable for comparisons between measured electron number

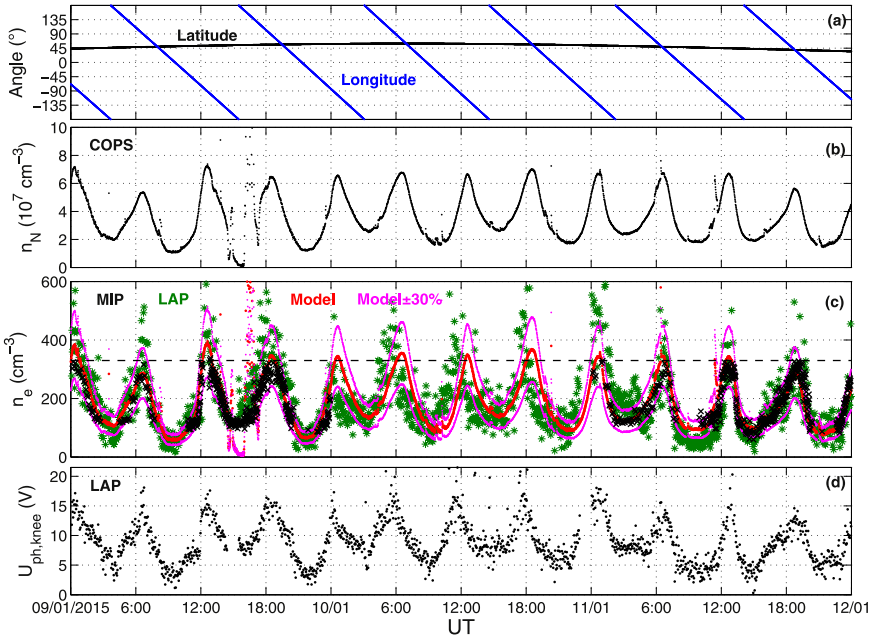

Figure 1. Shown vs. time are the following. (a) The latitudinal (black) and longitudinal (blue) coverage of *Rosetta*. (b) Neutral number densities measured by ROSINA/COPS. (c) Modeled and observed electron number densities. The modeled values shown in red are proportional to the ROSINA/COPS derived neutral number densities via Equation (1) with $r = 28$ km and with values of u and ν_{ph} as specified in Section 2.1. Electron number densities derived from RPC/MIP (RPC/LAP) are shown with black crosses (green asterisks). The dashed line marks the electron density detection upper limit of the RPC/MIP experiment when operated in the Long Debye Length mode (MIP-LDL). (d) Photoelectron-knee potential derived from RPC/LAP.

densities and modeled values. During these dates the *Rosetta* spacecraft resided at northern latitudes (43°–58°) at a cometocentric distance of ∼28 km (the latitude and longitude coverage are shown versus time in Figure 1(a)). At this point, and until equinox in 2015 May, the northern side was the summer (and most active) side of the comet, with an outgassing largely dominated by H_2O in contrast to the southern side where an alternating dominance of H_2O and CO2 prevailed (Hässig et al. 2015; Le Roy et al. 2015). This justifies criterion (i) listed in Section 2.1 (i.e., the focusing on an H_2O dominated coma). Criterion (ii) is partly justified by the coma being optically thin to EUV irradiation (in fact all the way to the surface). Criterion (iii) is justified by the fact that the timescale for dissociative recombination is orders of magnitudes higher than the timescale for radial transport. In addition, due to the low activity we deem it unlikely that the charging of nanograins had a profound influence on the overall ionization balance (c.f. Vigren et al. 2015b). As for criterion (iv), we refer to Equation (10) of Gombosi (2015, pp. 169–188) stating that the cometocentric distance R_{IN}, where ions decouple from neutrals, can be approximated as:

$$R_{IN} \approx \frac{k_{IN} Q}{4\pi u^2} \approx \frac{k_{IN} r^2}{u} n_N(r), \quad (3)$$

where k_{IN} is the ion-neutral charge transfer collision frequency, Q is the molecular outgassing rate, and u is the expansion velocity of the neutrals. The latter equality follows from the assumption of a Haser-like outgassing ($n_N \approx Q/4\pi u r^2$). With u set to 0.53 km s^{-1} and $k_{IN} = 1.1 \times 10^{-9}$ cm^3 s^{-1} (as used by Gombosi 2015, pp. 169–188) the neutral number densities measured at $r = 28$ km (see Section 3.1) give R_{IN} estimates that are typically in the range ∼30–100 km. Our focus in this study is exclusively on $r \sim 28$ km, so the assumption that the ions have the same velocity as the neutrals therefore seems reasonable. However, Gombosi (2015, pp. 169–188) also noted that solar wind interactions can reduce the extent of the strongly coupled plasma. We make no attempt to account for such interactions in our calculations.

3. IN SITU MEASUREMENTS

3.1. Neutral Number Densities

The neutral number densities derived from ROSINA/COPS are shown versus time in Figure 1(b). For a description of ROSINA/COPS and its working principle we refer to Balsiger et al. (2007). The displayed data has been corrected for spacecraft background and the composition is assumed to be H_2O dominated. A spacecraft maneuver affected ROSINA/COPS measurements between ∼14.00 and 17.00 UT on January 9, so this time frame should be ignored when inspecting Figure 1(b). Similar as reported by Hässig et al. (2015) for 2014 August–September, the neutral number densities peak at longitudes within tens of degrees of ±90° when over the neck region and the maximum surface area is exposed to sunlight. The dips occur at longitudes within tens of degrees from ∼0° and ±180° when viewing the smaller and the larger of the lobes, respectively.

3.2. Electron Number Densities

The electron number densities $n_{e,MIP}$ derived from RPC/MIP Long Debye Length (LDL) mode are shown with black crosses in Figure 1(c). The RPC/MIP instrument and its working principle are described in detail in Trotignon et al. (2007) and references therein. The electron number densities are derived from the estimated position of the plasma frequency in the MIP complex (amplitude and phase) mutual impedance spectra. The displayed data are median values over 30 consecutive density estimates at a cadence of ∼10 s or ∼3 s,

depending on the time of the day (normal and burst modes, respectively). MIP did not operate in LDL mode during January 10.

Note that the plasma density retrieved when using the LDL mode of the MIP experiment is limited at both high and low number densities. First, with the frequency range being limited to [7–168] kHz in the LDL operational mode, plasma densities higher than $\sim 350\,\mathrm{cm}^{-3}$ are not observable (the dashed line in Figure 1(c) is drawn at $330\,\mathrm{cm}^{-3}$, which is just above the highest number densities extracted). Second, the mutual impedance spectra are typically flat in frequency (as expected in vacuum) when the distance between the electric emitters and the receivers is much larger than the Debye length. This implies that the MIP experiment is not sensitive to plasmas with a small enough number density (i.e., a large enough Debye length, depending on the electron temperature). In the case of ~5 eV electrons (as suggested by LAP observations), these lower threshold is around 30–50 cm^{-3}. Due to these limitations and to the high variability of the cometary plasma density at short timescales compared to the timescales of interest in this study, it is stressed that at times when the plasma frequency is not observed in a significant fraction of consecutive recordings, the extracted median values could significantly either under- or overestimate the actual average electron number density. Biased median values based on less than a third of consecutive estimated plasma frequencies are excluded from the data shown in Figure 1(c).

The green asterisks in Figure 1(c) show electron number densities derived from RPC-LAP bias voltage sweeps using the LAP1 sensor. These values have been derived from the slope of the current-voltage relation in the electron attraction region (positive probe voltage with respect to the plasma), assuming a constant electron temperature of $T_e = 5$ eV. An automated analysis of T_e gives values scattered in the 3–7 eV range, but because a significant part of this spread can be due to dynamics, we prefer to use a mean value. We thus get a value for the density that is a factor $\sqrt{T_e\,[\mathrm{eV}]/5}$ off from the real value, meaning up to 30% for T_e in the indicated range, which is clearly smaller than the range of density variation observed. The density has been further adjusted by a Boltzmann factor to correct for the depletion of electrons in the vicinity of the negative spacecraft potential (Odelstad et al. 2015). The resulting values give good overlap with the MIP-LDL data not only for January 9 and 11, but also for other close-by dates. Primarily because it is sampling a larger volume, RPC/MIP (when operated in the LDL mode) is expected to be less sensitive than RPC/LAP to the decay of the spacecraft potential.

4. RESULTS AND DISCUSSION

4.1. Comparison Between Observed and Modeled Electron Number Densities

Modeled electron number densities (derived from n_N and Equation (1) and shown by the red line in Figure 1(c)) are in reasonably good agreement with the observed values throughout the investigated time period (excluding the 14.00–17.00 UT interval on January 9, where the spacecraft maneuver affected the ROSINA/COPS measurements). Figure 1(c) shows that the bulk of the $n_{e,MIP}$ data set, as well as the bulk of the $n_{e,LAP}$ data set, is located within ±30% of $n_{e,Model}$ (the magenta colored lines in Figure 1(c) are drawn at ±30% of $n_{e,Model}$). We also note a good agreement between $n_{e,MIP}$ and $n_{e,Model}$. During the neutral number density dip from about 8.00 to 11.00 UT on January 11, and periodically also during January 10, $n_{e,LAP}$ data are lower than modeled values by about 50%.

The good level of agreement—prevailing most of the time between modeled and observed electron number densities—*indicates* the validity of the central underlying assumptions in the FFCF model during the investigated time period. To prove this more rigorously requires a follow-up investigation invoking all instruments within the RPC, but some lines of thoughts are worth addressing at this point. At first sight, an obvious issue with the assumption of radial expansion may be magnetic field effects, because no diamagnetic cavity had formed (or been observed) at this stage of *Rosetta*'s investigation of 67P (Goetz et al. 2016). As a typical local value of the magnetic field strength at this stage of cometary activity we assume 10–15 nT, which is consistent with observations a few weeks before and prior to the impact of a solar wind event (Edberg et al. 2016). An H_2O^+ (or H_3O^+) ion at the flow speed of $500\,\mathrm{m\,s}^{-1}$ then has a gyroradius around 7–10 km. For comparison, using an ion-neutral collision cross-section $\sim 4 \times 10^{-14}\,\mathrm{cm}^2$ (based on Fleshman et al. 2012, assuming collision energies near or below 0.1 eV) the ion collision mean free path is ~5 km at the position of *Rosetta* for a neutral density of $5 \times 10^7\,\mathrm{cm}^{-3}$. Because the neutral density varies as $1/r^2$, the collisionality increases rapidly as we look farther in toward the nucleus. Magnetic field effects on the cometary ions are thus, at most, marginal at our distance (and less important for ions transported from inside). This is in line with the present results and also partially verified by Edberg et al. (2015), who found an $1/r$ plasma density profile fitting LAP data quite well, albeit with large variations, as far out as 250 km during an excursion to that distance a month after the case studies of this paper. Nevertheless, it is clear that for detailed modeling of the region where the gyroradius is below the collision length and gradient scale of the plasma, our radial expansion assumption for the plasma would fail, requiring more complex models including the magnetic field, and we may be on the limit of its applicability.

Recorded electron and ion spectrograms from the RPC/IES and the RPC/ICA instruments can be used to estimate *ambient* electron impact ionization frequencies and solar wind charge exchange frequencies. However, the ambient relative importance of different ion/ionization sources is not necessarily reflecting the origins of the ambient ion population (within the FFCF model the ion population at cometocentric distance r originates along the line toward the nucleus with equal contribution from all distances). Both IES and ICA can measure the energy distribution and flow directions of ions. Measurements by the instruments revealed, for example, significant deflection of solar wind ions even at low cometary activity (Broiles et al. 2015; Nilsson et al. 2015). For the cometary ions with a spacecraft potential in the range −20 to −10 V, however, it *may* present a challenge to tell whether the "low-energy ions" in the absence of the spacecraft would fly with a velocity near the neutral bulk velocity or to be elevated in speed by a few $\mathrm{km\,s}^{-1}$ (or for that matter be nearly stagnated). Below we propose an alternative approach to further test the assumption of a radially expanding plasma with $u_I \approx u_N$.

4.2. The H_3O^+/H_2O^+ Number Density Ratio and its Relation to the Ion Expansion Speed

The ROSINA/DFMS (Balsiger et al. 2007; Fuselier et al. 2015) can be used to derive the relative abundances within the cometary ion population. Under the assumption of a constant ionization frequency and that produced ions move radially outward at the same speed as the bulk of the neutral flow, it is possible to derive an analytical expression for the H_3O^+/H_2O^+ number density ratio. For this we make the additional assumption that dissociative recombination is inefficient and that the coma is dilute enough such that the prevalence at low mixing ratios of high proton affinity molecules (e.g., NH_3 and CH_3OH) does not cause a rapid loss of H_3O^+ ions.

As justified by simulations, the principal processes dictating the H_2O^+ and H_3O^+ ion number densities are the photoionization of H_2O (yielding primarily H_2O^+) and the proton transfer reaction $H_2O^+ + H_2O \rightarrow H_3O^+ + OH$. The reduced version of the continuity equation for H_2O^+ (an ion that is indexed as 18) becomes

$$\frac{u_N}{r^2}\frac{\partial}{\partial r}(r^2 n_{18}) = n_N(r) \times (\nu - k n_{18}), \quad (4)$$

where n_N is the water number density at r, u_N is the radial speed of the coma constituents, ν is the partial ionization frequency of H_2O yielding H_2O^+, and k is the rate coefficient for the proton transfer reaction $H_2O^+ + H_2O \rightarrow H_3O^+ + OH$. A value of $k = 2.1 \times 10^{-9}\,cm^3\,s^{-1}$ was experimentally determined at room temperature by Huntress & Pinizzotto (1973).

Because we focus on distances close to the nucleus, the neutral number density n_N is inversely proportional to u_N and r^2, and Equation (4) can be rewritten in the form

$$\frac{\partial}{\partial r}(r^2 n_{18}) = \frac{C}{u_N^2} \times (\nu - k n_{18}), \quad (5)$$

where we introduced $C = n_N r^2 u_N$. Differentiating and rearranging gives the inhomogeneous differential equation

$$\frac{\partial}{\partial r} n_{18} + \left(\frac{2}{r} + \frac{Ck}{u_N^2 r^2}\right) n_{18} = \frac{C\nu}{u_N^2 r^2}, \quad (6)$$

that with the boundary condition $n_{18}(r = r_C) = 0$ (implying that there are no ions in the vicinity of the surface at a cometocentric distance of r_C) has the solution

$$n_{18}(r) = \frac{n_N \nu}{u_N}(r - r_C \exp\{\eta r - \eta r^2/r_C\} + \eta r^2 \exp(\eta r)\{E_n(\eta r^2/r_C) - E_n(\eta r)\}), \quad (7)$$

where we have implemented to the "raw" solution the relation $n_N = C/u_N r^2$ and introduced the parameter

$$\eta = \frac{n_N k}{u_N}. \quad (8)$$

The function E_n in Equation (7) is the exponential integral function (available as expint() in Matlab™) and defined as

$$E_n(x) = \int_x^\infty \frac{e^{-t}}{t} dt. \quad (9)$$

Because the loss of H_2O^+ in this simplified treatment is always associated with the production of H_3O^+ (an ion that below is indexed as 19) we can express

$$\frac{n_{19}}{n_{18}} = \frac{n_{19} + n_{18}}{n_{18}} - 1. \quad (10)$$

The total number density of H_2O^+ and H_3O^+ is the same as the H_2O^+ number density from a calculation in which one switches off the proton transfer channel. This is readily obtained (by integrating ion production from r_C to r) as

$$n_{19} + n_{18} = \frac{(r - r_C)\nu n_N}{u_N}. \quad (11)$$

Combining (7), (10), and (11) gives as a guiding expression, $G19/18$, of the H_3O^+ to H_2O^+ number density ratio:

$$G_{19/18}(r, n_N) = \frac{r - r_C}{r - r_C \exp\left\{\eta r - \frac{\eta r^2}{r_C}\right\} + \eta r^2 \exp(\eta r)\left\{E_n\left(\frac{\eta r^2}{r_C}\right) - E_n(\eta r)\right\}} - 1, \quad (12)$$

with η according to Equation (8) and with E_n being the exponential integral function. A simpler expression arises when H_2O^+ is under photochemical equilibrium (with the left-hand side of Equation (4) equal to zero):

$$G^*_{19/18}(r, n_N) = \frac{(r - r_C) k n_N}{u_N} - 1. \quad (13)$$

In Figure 2 we plot $G_{19/18}$ (Equation (12)) as a function of r for various local outgassing rates (the different runs correspond to neutral number densities at $r = 28$ km of $1 \times 10^7\,cm^{-3}$, $3 \times 10^7\,cm^{-3}$, and $6 \times 10^7\,cm^{-3}$, respectively, with the use of $u_N = 0.52\,km\,s^{-1}$). For comparison, we also show the associated results from an ion-neutral chemistry model adopted from Vigren & Galand (2013), but adjusted to consider a pure H_2O coma and photoionization as the only mechanism of electron-ion pair formation. Equation (12) reproduces well the results from the numerical simulation. The ratios derived from the numerical model, which account for OH^+, H^+, and O^+ production and reactions of these species with H_2O, exceed the values from Equation (12), but only by ~12%–20%. The use of Equation (13) gives H_3O^+/H_2O^+ ratios at $r = 28$ km that in comparison to values derived from Equation (12) are lower by 96%, 43%, and 24% for simulations in which $u_N = 0.52\,km\,s^{-1}$ and in which the neutral number density at $r = 28$ km is $1 \times 10^7\,cm^{-3}$, $3 \times 10^7\,cm^{-3}$, and $6 \times 10^7\,cm^{-3}$, respectively.

Note that $G_{19/18}$ (and the simpler $G^*_{19/18}$) in contrast to $G_{e/N}$ is independent of the ionization frequency, so we propose that comparisons between observed H_3O^+/H_2O^+ ratios with values given by Equation (12) can be used to get further hints on the bulk motion of the ion population. Observed ratios that are markedly lower than $G_{19/18}$ would, for example, speak in favor of the presence of ion acceleration along electric fields (reducing the efficiency of ion-neutral chemistry); other explanations for discrepancies may commence and are discussed briefly in Section 4.3. Fuselier et al. (2015) compared H_3O^+/H_2O^+ derived from a numerical simulation (driven by ROSINA/COPS observations of the neutral number density) with ratios observed by the ROSINA/DFMS during 2014 November 20, 23, 27, and 29 and 2014 December 2 (their simulation results are reproduced within ~15% by

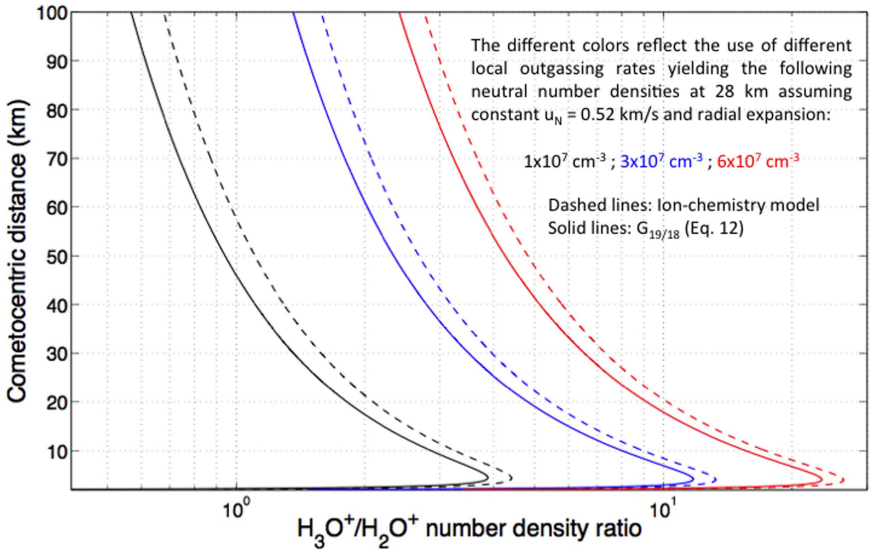

Figure 2. Comparison between the H_3O^+/H_2O^+ number density ratios derived from the field free ion chemistry model (dashed lines) and the analytical expression given by Equation (12) (solid lines). The different colors represent different local outgassing rates. The radial expansion speed was set to 0.52 km s^{-1}. The branching fractions for the photoionization of H_2O were set to 70.3%, 19.7%, 8.8%, and 1.2% for production of H_2O^+, OH^+, H^+, and O^+, respectively. The utilized rate coefficients for ion–H_2O reactions were adopted from Vigren & Galand (2013) and formation of cluster-ions was neglected. The electron temperature affecting dissociative recombination rate coefficients was set to 50,000 K (~5 eV).

Equation (12) when using similar values of u_N and k) when at a cometocentric distance of ~30 km. The model–observation comparisons by Fuselier et al. (2015) were not made exclusively for northern latitudes and mostly at ambient neutral number densities of $\sim 1 \times 10^7$ cm^{-3}, where typically the modeled values exceeded observations by more than a factor of 2 (see their Figure 7). On the contrary, for the single comparison made when the neutral number density was close to 3×10^7 cm^{-3}, a good agreement with modeled results was seen. We foresee further ROSINA/DFMS-derived H_3O^+/H_2O^+ number density ratios, especially in strongly H_2O dominated regions and moderately active phases.

4.3. Other Aspects Possibly Affecting the H_3O^+/H_2O^+ Number Density Ratio

H_3O^+/H_2O^+ ratios (as well as the electron number density) would be affected by a cometary plasma flow pattern in the near nucleus environment that is more complex than described by a simple radial outflow at constant velocity (for MHD and hybrid model results of plasma flow patterns around weakly outgassing comets, see, e.g., Rubin et al. 2012, 2014; Koenders et al. 2013, 2015). For example, in regions with slow moving or nearly stagnated ions, H_2O^+ ions could be subject to conversion to H_3O^+ ions, leading to enhanced H_3O^+/H_2O^+ number density ratios. In the following we only follow the scenario with ions flowing radially outward with the same speed as the neutrals, and discuss some further aspects that may influence H_3O^+/H_2O^+ number density ratios.

In the derivation of Equations (12) and (13) we assumed a constant ionization frequency along the nucleus-spacecraft line. This is a good approximation for the photoionization (attested from models of the attenuation of the impinging solar EUV flux, see, e.g., Vigren et al. 2015a), but the same may not hold for the electron impact ionization frequency. In the scenario of a radially expanding plasma, a pronounced decreasing effect on H_3O^+/H_2O^+ ratios would require the electron impact ionization frequency to be at least comparable with the photoionization frequency near the spacecraft, and that its relative importance drops toward the nucleus (Galand et al. 2016). This yields an enhanced production of H_2O^+ ions near the spacecraft, which have higher probabilities of avoiding proton transfer on their journeys toward the spacecraft than ions formed in higher density regions closer to the nucleus.

The neglect of dissociative recombination when deriving $G_{19/18}$ is fine for the considered activity levels. When within our one-dimensional model, invoking an unrealistically low electron temperature of 20 K along the nucleus-spacecraft line (e.g., note that LAP measures electron temperatures of 3–7 eV at the spacecraft location), enhancing the recombination rates of H_2O^+ and H_3O^+, which are proportional to $T_e^{-0.5}$ and $T_e^{-0.83}$, respectively (see Vigren & Galand 2013 and references therein), the resulting H_3O^+/H_2O^+ ratios at $r = 28$ km from the numerical ionospheric model drop only by ~2%, ~5%, and ~9% for the three activity levels considered in Section 4.2. In each case the drops reflect essentially only reduced H_3O^+ number densities, implying that for H_2O^+ the loss rate due to dissociative recombination remains negligible in comparison to its loss rate associated with transport and proton transfer to H_2O. The predicted H_3O^+/H_2O^+ ratios are severely more sensitive to variations in the rate coefficient, k, used for the reaction $H_2O^+ + H_2O \rightarrow H_3O^+ + OH$. Due to the polar nature of the water molecule, k is expected to have a negative temperature dependence and, e.g., be higher by ~70% at temperatures of 100 K compared with 300 K (see, e.g., Vigren & Galand 2013); this reflects nearly linearly in the predicted H_3O^+/H_2O^+ ratios when assuming constant temperature profiles. In more active stages both dissociative recombination and proton transfer from H_3O^+ to neutrals with higher proton affinity than H_2O have a greater influence on the H_3O^+/H_2O^+ number density ratios and needs to be accounted for.

5. SUMMARY AND CONCLUDING REMARKS

During 2015 January 9–11, the *Rosetta* spacecraft swept northern latitudes (at that time the summer and most active

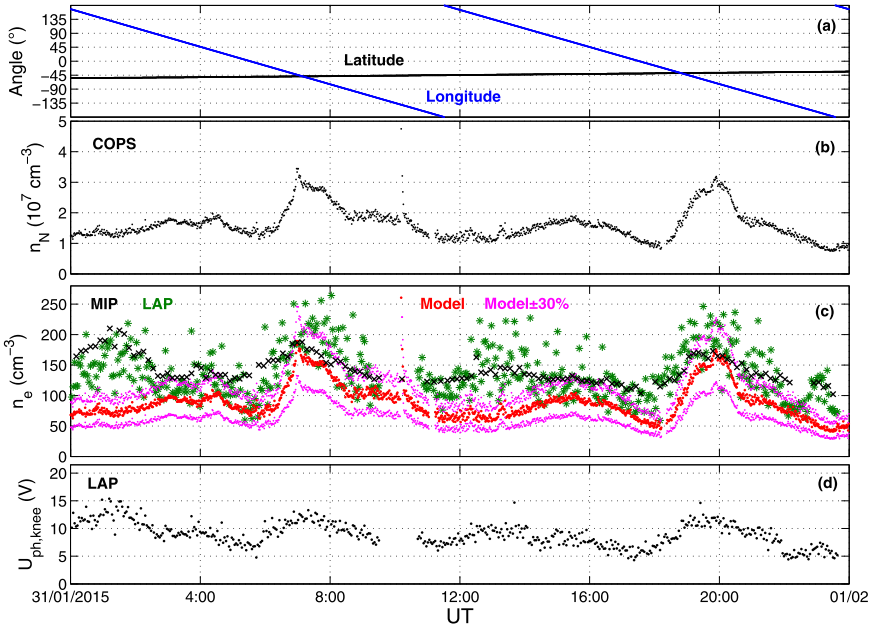

Figure 3. Same as in Figure 1, but with data from 2015 January 31 when *Rosetta* resided at southern latitudes (cometocentric distance of ∼28 km and heliocentric distance of ∼2.41 au).

side) of 67P at a cometocentric distance of ∼28 km (the heliocentric distance was ∼2.58 au). We have shown that for these dates the electron number densities derived from a simple FFCF model driven by neutral number densities derived from ROSINA/COPS measurements reproduce well the electron number densities measured by RPC/MIP and RPC/LAP.

The good level of agreement between the modeled and observed electron number densities is an indication (but not a standalone proof) for the validity of the most critical assumptions in the model (see Section 2.1). We note especially that the assumption of $u_I \approx u_N$ (ion velocity ≈ neutral velocity) seems reasonable for the investigated time period and for cometocentric distances smaller than the spacecraft-nucleus separation. This is in line with the idea that the ion-neutral decoupling distance is estimated from simplified theory to be in the vicinity of (or longer than) the nucleus-spacecraft distance for the considered time period (see Section 2.1). To understand how the decoupling distance is affected by the interplay between the coma and the solar wind requires sophisticated hybrid and/or MHD modeling (e.g., Koenders et al. 2013, 2015; Rubin et al. 2014). We have noted that studies using the full RPC instrument set can eventually give a more complete picture of the processes dictating the ionization balance. We also proposed that ROSINA/DFMS measurements of H_3O^+/H_2O^+ number density ratios can be used as an independent indicator for the validity of the $u_I \approx u_N$ assumption (see Section 4.2).

We emphasize that the good level of agreement between the modeled and observed electron number densities reported here are for a limited three-day period in 2015 January when at northern latitudes and when close to the nucleus ($r \sim 28$ km). A similar good agreement is found for 2015 January 21 (not shown; data coverage from 14.00 UT and onward), again when at northern latitudes and with similar cometocentric distance. For southern latitudes at nearby dates, the picture is much different—modeled electron number densities, often over hour long periods, exceed the observed electron number densities by more than a factor of 2, while at other times are in good agreement. This is illustrated in Figure 3, which is organized the same way as Figure 1, but with data from 2015 January 31, when at a heliocentric distance of 2.41 au and a cometocentric distance of 28 km. It is noted that the good level of agreement in the model–observation comparison is seen at times when over the neck region and when the neutral number densities peaks. Worse agreement is seen for longitudes near 0° and 180°. We propose that the alternating level of agreement between the modeled and observed electron number densities may result, at least partly, from an alternating dominance of CO_2 and H_2O (Hässig et al. 2015) and therefore spatially varying effective ionization frequencies and expansion speeds (not considered in the model).

Rosetta is a European Space Agency (ESA) mission with contributions from its member states and the National Aeronautics and Space Administration (NASA). Work at the Swedish Institute of Space Physics is supported by the Swedish National Space Board (SNSB; contract numbers 109/02, 114/13, 135/13, 166/14) and by the Swedish Research Council (contract numbers 621-2013-4191 and 621-2014-5526). Work at the University of Bern on ROSINA/COPS was funded by the State of Bern, the Swiss National Science Foundation, and the European Space Agency PRODEX Program. M.G. is partially funded by the Science & Technology Facilities Council (STFC) through grant ST/K001051/1 to Imperial College London. Work at LPC2E/CNRS was supported by CNES and ANR under the financial agreement ANR-15-CE31-0009-01. We thank Tom Woods (the PI of the TIMED/SEE) and his team for providing solar EUV fluxes and we thank an anonymous reviewer for valuable comments.

REFERENCES

Balsiger, H., Altwegg, K., Bochsler, P., et al. 2007, SSRv, 128, 745
Bieler, A., Altwegg, K., Balsiger, H., et al. 2015, A&A, 583, A7
Biver, N., Hofstadter, M., Gulkis, S., et al. 2015, A&A, 583, A3

Broiles, T., Burch, J. L., Clark, G., et al. 2015, A&A, 583, A21
Burch, J., Goldstein, R., Cravens, T. E., et al. 2007, SSRv, 128, 697
Carr, C., Cupido, E., Lee, C. G. Y., et al. 2007, SSRv, 128, 629
Cochran, A. L., & Schleicher, D. G. 1993, Icar, 105, 235
Edberg, N. J. T., Eriksson, A. I., Odelstad, E., et al. 2015, GeoRL, 42, 4263
Edberg, N. J. T., Eriksson, A. I., Odelstad, E., et al. 2016, JGR, 121, 949
Eriksson, A. I., Boström, R., Gill, R., et al. 2007, SSRv, 128, 729
Fleshman, B. L., Delamere, P. A., Bagenal, F., & Cassidy, T. 2012, JGR, 117, E05007
Fuselier, S., Altwegg, K., Balsiger, H., et al. 2015, A&A, 583, A2
Galand, M., Héritier, K. L., Odelstad, E., et al. 2016, submitted
Glassmeier, K.-H., Richter, I., Diedrich, A., et al. 2007, SSRv, 128, 649
Goetz, C., Koenders, C., Richter, I., et al. 2016, A&A, 588, A24
Gombosi, T. I. 2015, Physics of Cometary Magnetospheres, in Magnetotails in the Solar System (Hoboken, NJ: John Wiley & Sons, Inc.)
Hässig, M., Altwegg, K., Blasiger, H., et al. 2015, Sci, 347, 0276
Huntress, W. T., & Pinizzotto, R. F. 1973, JCP, 59, 4742
Koenders, C., Glassmeier, K.-H., Richter, I., et al. 2013, P&SS, 87, 85
Koenders, C., Glassmeier, K.-H., Richter, I., et al. 2015, P&SS, 105, 101
Lamy, P. I., Toth, I., Davidsson, B. J. R., et al. 2007, SSRv, 128, 23
Le Roy, L., Altwegg, K., Balsiger, H., et al. 2015, A&A, 583, A1
Massironi, M., Simioni, E., Marzari, F., et al. 2015, Natur, 526, 402
Nilsson, H., Lundin, R., Lundin, K., et al. 2007, SSRv, 128, 671
Nilsson, H., Stenberg Wieser, G., Behar, E., et al. 2015, A&A, 583, A20
Odelstad, E., Eriksson, A. I., Edberg, N. J. T., et al. 2015, GeoRL, 42, 10126
Rubin, M., Hansen, K. C., Combi, M. R., et al. 2012, JGR, 117, A06227
Rubin, M., Koenders, C., Altwegg, K., et al. 2014, Icar, 242, 38
Schunk, R. W., & Nagy, A. F. 2009, Ionospheres: Physics, Plasma Physics & Chemistry (Cambridge: Cambridge Univ. Press)
Sierks, H., Barbieri, C., Lamy, P. L., et al. 2015, Sci, 347, 1044
Trotignon, J. G., Michau, J. L., Laboutte, D., et al. 2007, SSRv, 128, 713
Vigren, E., & Galand, M. 2013, ApJ, 772, 33
Vigren, E., Galand, M., Eriksson, A. I., et al. 2015a, ApJ, 812, 54
Vigren, E., Galand, M., Eriksson, A. I., et al. 2015b, ApJ, 798, 130
Woods, T. N., Eparvier, F. G., Bailey, S. M., et al. 2005, JGR, 110, A01312